Predictive Control of Surface Roughness as a Function of Temperature in a SiN_x Thin Film Deposition Process Using the Kinetic Monte Carlo Method

A. Bouhadiche[a,*], S. Benghorieb[a], H. Bouridah[b,c], M.R. Beghoul[b,c], R. Remmouche[b,c] and H. Haoues[b,c]

[a]*Research Unit in Optics and Photonics (UROP), Center for Development of Advanced Technologies (CDTA), Setif 19000, Algeria*
[b]*Department of Electronics, University of Jijel, BP98, Ouled Aissa, Jijel 18000, Algeria*
[c]*Materials Study Laboratory, University of Jijel, BP98, Ouled Aissa, Jijel 18000, Algeria*

Received: 07.08.2024 & Accepted: 04.02.2025

Doi: 10.12693/APhysPolA.147.333 *e-mail: a.bouhadiche@gmail.com

Silicon nitride (SiN_x) films are crucial in microelectronic and photonic devices, where their interface affects performance and reliability. In this study the effect of deposition temperature on the surface roughness of amorphous SiN_x films on silicon (Si) substrates is investigated using our kinetic Monte Carlo algorithm (*Silicon* **15**, 5209 (2023)). The low-pressure chemical vapor deposition process is modeled on a three-dimensional triangular lattice with disilane (Si_2H_6) and ammonia (NH_3) as precursor sources. The nanoscopic events included in this work are the nanoparticle adsorption and the Si adatom migration. A new growth model is adopted to control the obtained surface morphologies, i.e., size and density of amorphous Si clusters as well as film surface roughness. The deposition of Si and N atoms is carried out alternately to create a SiN compound characterized by small Si clusters and a rough surface. Both volume migration and surface migration are taken into account during the simulation, leading to the development of vacancies and pores. The formation of peaks and valleys is described by our kinetic Monte Carlo algorithm. Our analysis includes deposition simulations at temperature values ranging from 723 to 753 K, with a gas flow rate fixed at 0.3 and a deposition duration of 1 h. The surface roughness values of the deposited nanostructures are deduced from the simulation matrix. Numerical results indicate that an increase in process temperature leads to an increase in the size of Si clusters along with an increase in surface roughness. The deposition temperature largely determines whether the film surface is smooth or rough. This means that our growth model is able to accurately predict the evolution of the film nanostructure for a wide range of process conditions. The stoichiometry x (N/Si ratio) is determined based on all deposition parameters. The average distance between Si clusters is also calculated here. The acquired insights enable the refinement of thin film deposition simulation techniques, the improvement of surface morphology properties, and the support of the development of reliable SiN platforms for microelectronics and photonics.

topics: silicon nitride, kinetic Monte Carlo (KMC), deposition temperature, surface roughness

1. Introduction

Silicon nitride (SiN_x) is an important dielectric that has attracted considerable research attention over the past decades in the field of fabrication of optoelectronic and microelectronic semiconductor devices [1–5]. SiN_x exhibits peculiar optical, electrical, mechanical, and thermal properties, such as high dielectric constant with a wide transparency window from visible to mid-infrared wavelengths, optical band gap, critical electrical insulation, anti-oxidation, high strength, crucial fracture toughness, good heat and corrosion resistance, and high thermal conductivity [6–11]. The composition and properties of silicon nitride films can be tuned by varying the synthesis parameters [12–18].

SiN_x has been widely used in many optical components and applications, such as antireflection coatings [19–21], surface passivation layers in silicon solar cells [22, 23], thin film transistors (TFT) [24, 25], photoluminescence enhancement [26, 27], surface-enhanced Raman spectroscopy [28, 29], imaging applications [30, 31], integrated optics [32, 33], and metamaterials [34, 35]. It is of great interest for chemical and biological detection [36–41]. Moreover, the low leakage of SiN_x makes it the best candidate for barrier layers of organic light-emitting diodes (OLEDs) [42, 43].

To obtain SiN_x thin films, several kinds of technologies can be used: physical vapor deposition (PVD) [44], DC magnetron sputtering [45], plasma-enhanced chemical vapor deposition (PECVD) [46], catalytic chemical vapor deposition (Cat-CVD) [47], and low-pressure chemical vapor deposition (LPCVD) [48, 49]. LPCVD is preferred over other techniques for its ability to produce high-quality films. This synthesis method depends on high temperatures to promote chemical reactions on the substrate surface, according to precursor flow rates and deposition duration. It uses low deposition kinetic energy, contrary to plasma-based techniques, which reduces the effects of atomic bombardment and ensures the occurrence of surface reactions. However, the integration of SiN_x into complex systems still suffers from many challenges, such as compatibility issues: residual stress [50–52], cracking risk [53, 54], and defect generation during the fabrication process [55]. These challenges highlight the importance of understanding the growth mechanisms and properties of SiN_x films.

To fill this gap, our research focuses on investigating the effect of substrate temperature on the morphological properties of SiN_x thin films obtained by the LPCVD technique on silicon (Si) substrates with a mixture of disilane (Si_2H_6) and ammonia (NH_3) as precursor sources. The deposition process is modeled via our kinetic Monte Carlo (KMC) algorithm [56] on a three-dimensional triangular lattice. Two nanoscopic events are considered in this work, namely the adsorption of nanoparticles (NPs) and the subsequent migration, which influence the surfaces of the deposited films. A new method is adopted to define the film surface roughness from the simulation matrix. By specifying all input parameters, the structures of the deposited films in terms of Si cluster size and surface roughness can be studied by varying the process temperature values. This comprehensive approach aims to prove if this critical parameter enables determining the surface of the film, whether it is smooth or rough. The average distance between Si clusters is defined. The proportion of Si and N atoms in the final thin film is established. This study provides a novel perspective in SiN_x film research, contributing to the optimization of microelectronic and photonic devices.

2. Surface roughness model for kinetic Monte Carlo simulations of the SiN_x thin film LPCVD process

2.1. SiN_x LPCVD process mechanisms

Silicon nitride (SiN_x) thin films deposited on silicon substrates are simulated using the KMC method. A three-dimensional triangular rigid lattice $\tilde{M}$ ($200 \times 200 \times 200$ sites), where the deposition process takes place, is used. All deposits are located at discrete positions within the simulation lattice. The first two dimensions — x and y — correspond to the surface plane; the third — z — is the direction of growth. All elements of the matrix are defined with different values as follows:

- $\tilde{M}(i,j,k) = 0$ — empty site;
- $\tilde{M}(i,j,k) = 1$ — silicon adatom;
- $\tilde{M}(i,j,k) = 3$ — nitrogen adatom.

Two different types of nano-mechanisms are considered, namely the adsorption mechanism and the migration mechanism. In the adsorption mechanism, incident NPs are incorporated into the thin film with a rate given by the following expression [57]

$$V_d = V_{d_0} \exp\left(-\frac{E_a}{k_B T}\right), \tag{1}$$

where V_{d_0} is a pre-exponential factor, T is the process temperature, k_B is the Boltzmann constant, and E_a is the deposition activation energy estimated to be 217 kJ/mol [58].

The NP migration modeling approach indicates that Si adatoms are able to diffuse vertically from upper to lower regions, unlike our previous two-dimensional simulation model [59], where adatom diffusion is limited to the surface. A randomly selected unstable Si adatom (x, y, z), designated as 1, jumps against the appropriate energy barrier and moves to its most stable vacant neighbor site, 2, to lose its energy, with a migration probability

$$P_{1-2} = \min\left[1, \exp\left(-\frac{(F_2+F_{s2}) - (F_1+F_{s1})}{k_B T}\right)\right], \tag{2}$$

where $F = -\gamma n$; γ denotes the bond energies of an Si adatom and n the number of its bonds. The bond strengths γ of Si–Si and Si–N bonds at 298 K are 325 ± 7 and 470 ± 15 kJ/mol, respectively [60]. The energy function F is estimated to be equal to 0 when the number of bonds n becomes less than the critical number n_c ($n \leq n_c$, $n_c = 3$). For the 1st layer, the Si adatom–substrate binding energy F_s is taken as $-6\gamma_s$ ($\gamma_s = \gamma_{Si-Si}$, the deposition is carried out on a silicon substrate), while for the upper layers, $\gamma_s = \gamma_{Si-Si}$ or γ_{Si-N}. Si adatoms moving on the upper terraces fall very easily to the bottom of the step and eventually integrate into a cluster; Si adatoms are unable to jump upwards.

The chemical reactions by which SiN_x films are deposited from Si_2H_6 and NH_3 [59] are:

$$Si_2H_6 \rightarrow SiH_2 + SiH_4, \tag{3}$$

$$SiH_2 + NH_3 \rightarrow SiH_3NH_2, \tag{4}$$

$$SiH_3NH_2 \rightarrow SiH_2NH + H_2, \tag{5}$$

$$SiH_2 \rightarrow Si + H_2, \tag{6}$$

$$SiH_2NH \rightarrow Si + N + \tfrac{3}{2}H_2. \tag{7}$$

2.2. Model description

Based on our previously proposed growth model [56], we performed kinetic Monte Carlo (KMC) simulations to determine the morphologies of the obtained films in terms of size and density of amorphous Si clusters as well as film surface roughness. Random numbers are used to choose landing sites for molecules (or radicals). The random selection of the first two numbers leads to determining the coordinates (x, y) of one of the two atoms of the deposited molecule. Then, according to the z column, the new atom is deposited at the first lowest site it encounters. To clarify further, there are no restrictions or conditions for depositing when the site is empty. Conversely, when the site is occupied, the deposition occurs alternately (see Fig. 1) to form a SiN compound with small Si clusters; therefore, an N atom must be deposited only on a Si atom, and so on. This results in seven possibilities for the second atom deposition, as shown in Fig. 2 — six sites are located around the first atom, while the seventh places the SiN compound in a vertical position. In fact, the second atom can be deposited on the first atom if these six sites are occupied, i.e., by vertical deposition. In the remaining cases, one of these six sites is chosen randomly. Deposition can be carried out if the selected site is empty; otherwise, a new site is chosen according to the clockwise rule (Fig. 3). The development of vacancies and pores can be ensured when the site under the second atom is empty, which allows for the creation of peaks and valleys in the structure depending on the film thickness and surface roughness, as illustrated in Fig. 4. The original in this model is taking into account the migration of vacancies and pores in volume during film growth.

In the proposed model, the formation of vacancies within the system is spontaneous. During the simulation, this process is considered as a parallel and complementary event to the Si adatom migration event (Fig. 4a). In fact, when a single Si adatom migrates to the first adjacent vacant site it encounters, automatically leaving behind a new empty site, it appears that sites are exchanged between it and that neighbor, thus promoting the movement of vacancies within the lattice. The new empty site is indicated in the simulation matrix $\tilde{M}$ by the number 0 and is considered as a vacancy during the simulations. During the calculation, the probability value of the formation of this vacancy is considered to be equal to the probability value of the migration of this Si adatom, which can be obtained using (2).

The N–N interaction is here prevented in favor of the formation of the required Si–N bonds in the presence of abundant Si–Si bonds (due to the dominance of the silicon population in the lattice), i.e., the N–N bond density is negligible (~ 0) compared to the Si–Si and Si–N bond densities in the simulations.

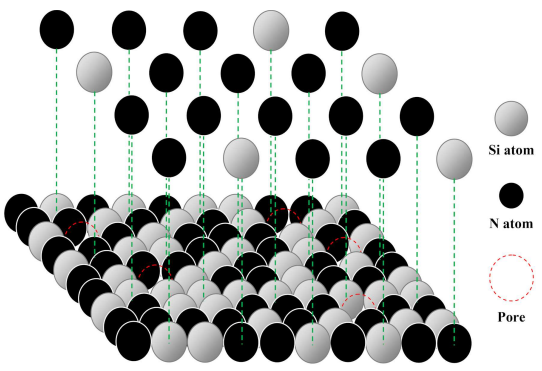

Fig. 1. Alternating deposition of NPs on a triangular matrix; Si (gray), N (black).

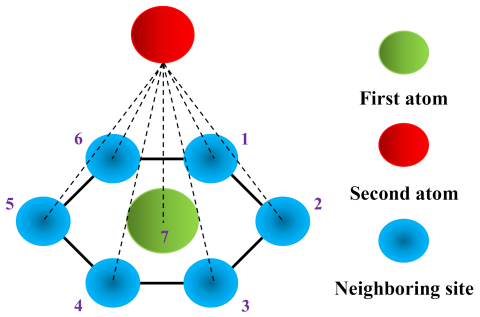

Fig. 2. The seven possibilities for the second atom deposition.

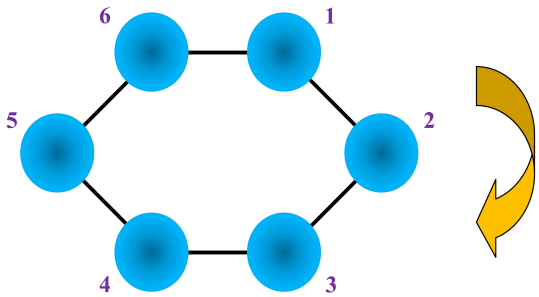

Fig. 3. A new site chosen according to the clockwise rule.

2.3. Surface roughness

Surface roughness R_m is generally used to describe the morphologies of deposited films and calculate the vertical deviation of the surface from a continuous flat surface [61, 62]. In our case, R_m is calculated from the simulation matrix; we take the first continuous film as a reference during simulations, as depicted in Fig. 5. We then count the number of sites occupied by atoms in each column. The

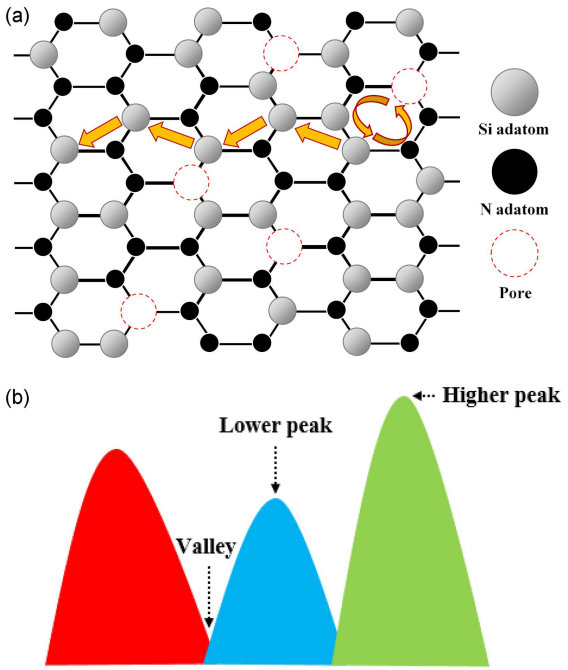

Fig. 4. (a) Migration of pores and vacancies in the SiN_x lattice and thus (b) creation of peaks and valleys.

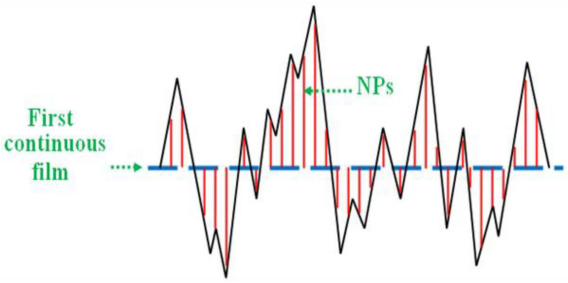

Fig. 5. Surface roughness calculation.

height of each column is obtained according to the diameters d of Si and N ($d_{\mathrm{Si}} = 0.25$ nm [63] and $d_{\mathrm{N}} = 0.184$ nm [64])

$$h\,(x,y) = N_h d, \tag{8}$$

where N_h is the number of layers at a given location (x,y). Finally, we average the heights of the existing columns in the simulation matrix

$$R_m = \frac{\sum h'\,(x,y)}{N}, \tag{9}$$

$$h'\,(x,y) = h\,(x,y) - h_{\min}, \tag{10}$$

where $h_{\min}$ is the lowest point on the surface (minimum film thickness) and the total number of surface sites is $N = 40\,000$ sites.

According to the proposed model, the deposited atoms are considered to be very close to each other, to the point that the distance between these atoms in front of their diameters can be neglected during the surface roughness calculation process.

2.4. Proposed KMC algorithm

Motivated by these considerations and assumptions, we can propose a KMC algorithm to predict and control the surface roughness as a function of temperature during LPCVD of SiN_x thin films on silicon substrates, as displayed in Fig. 6. First, we choose the initial parameters used during the simulations: matrix dimensions, pressure P, and deposition duration t_{KMC}. Afterward, the calculation of the probabilities of possible events is mandatory. At each KMC step, there is only one event to be executed, whether it is the deposition of a molecule or a radical or the migration of a Si adatom (the desorption mechanism is considered negligible, $P_{des} \sim 0$). The code then moves on to the next iteration until the deposit time is reached. Note that the selection of deposition sites is subject to the concepts and conditions included in the model proposed in Sect. 2.2. Two types of Si adatom migration are considered, namely in the volume and on the surface, which leads to a complementary event concerned with the evolution of pores and vacancies in the simulation matrix. At a given KMC step, a list of possible events is formed and updated. Each event l has a probability P_l calculated by dividing its frequency by the sum of all frequencies. The accumulation function is determined according to $R_{ac} = V_d + \sum r_m$; $r_m = r_1 + r_2 + r_3 + \ldots$ is the elementary migration rates. Probability P_l is confined between 0 and R_{ac}, as presented in Fig. 7. It seems that there is only one deposit event among dozens of different migration events. To identify the associated event type, i.e., whether it is an adsorption or migration event, a random number μ is generated as $\mu \in [0, R_{ac}]$. After the execution of the selected event, a second number σ is chosen arbitrarily as $\sigma \in [0,1]$ to update time with $t = t + \Delta t$, where $\Delta t = -\ln(\sigma)/R_{ac}$. Once the predefined deposition time is reached, we exit the loop by depositing a SiN_x film on a silicon substrate.

It is the process temperature T that determines whether the film surface is smooth or rough. For low T values, the formation of small Si clusters combined with the creation of Si–N bonds is favored, promoting rough surfaces. High T values result in a greater amount of energy to break the Si–N bonds and thus form large Si clusters due to the coalescence property, which encourages smooth surfaces.

3. Simulation results and discussion

We apply our growth model described above to study the LPCVD process of SiN_x thin films on silicon substrates using a mixture of Si_2H_6 and NH_3. Simulations of regulating film surface roughness are performed according to the deposition temperature T. The deposition process is carried out

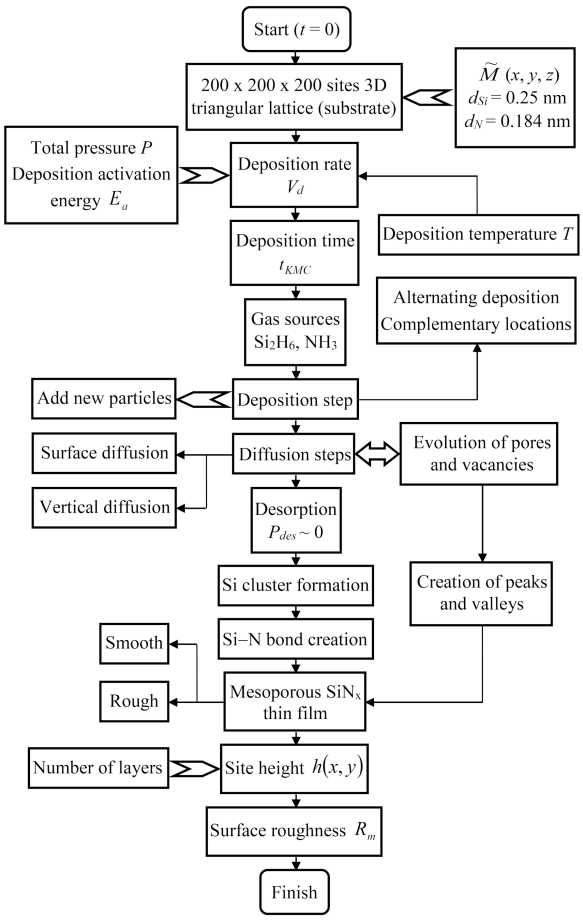

Fig. 6. Schematic diagram of the proposed KMC algorithm defining the substrate temperature control of the surface roughness of a LPCVD SiN_x thin film.

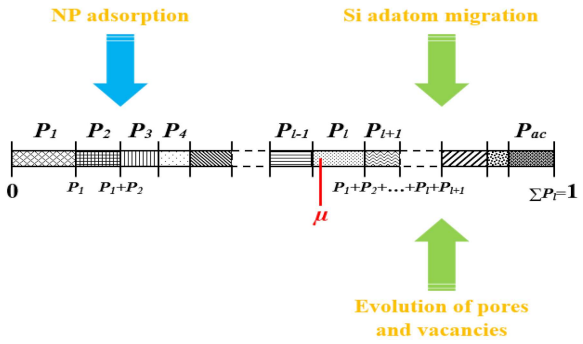

Fig. 7. List of possible events.

under a pressure P of 26.66 Pa [65, 66]. Three values of T are selected: 723, 738, and 753 K [58, 59], and we use the following input parameters [56]: matrix dimensions ($200 \times 200 \times 200$ sites), deposition time $t_{\mathrm{KMC}} = 1$ h, gas flow rate $R = 0.3$, and Si–N bond energy $E_{\mathrm{Si-N}} = 470$ kJ/mol. Note that the gas flow rate R is defined as $R = f(NH_3)/f(Si_2H_6)$, where $f(NH_3)$ is NH_3 flow and $f(Si_2H_6)$ is Si_2H_6 flow.

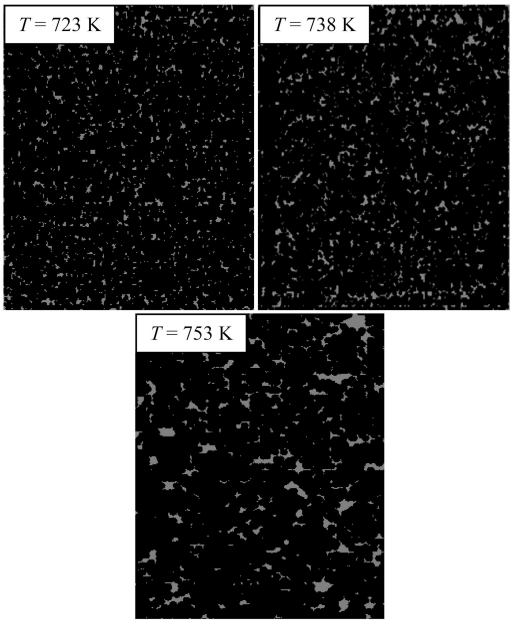

Fig. 8. Surface morphologies of SiN_x films for different T values.

Figure 8 explains well the correlation between the simulated surface morphologies of the deposited SiN_x films and the process temperature; the gray color refers to the amorphous Si clusters, unlike the black color, which corresponds to the regions occupied by nitrogen. To clarify, an increase in T allows for the development of amorphous Si cluster sizes combined with a decrease in their densities, as shown in Fig. 9. From an experimental point of view, larger Si clusters can be created at the threshold temperature value at which the energy required for NP coalescence overcomes the energy of the bonds formed between Si and impurities [67].

Figure 10 represents the variation of the average distance between Si clusters as a function of temperature. In fact, the increase in the temperature of the substrate leads to the deposition of nanostructures characterized by very close clusters. The distance between two clusters is defined as the distance between the two closest members or neighbors, according to the nearest neighbor method (single linkage method) [68]. As displayed in Fig. 11, one element $(x_1, y_{1,\max})$ from cluster 1 is selected along with its nearest element $(x_2, y_{2,\min})$ from cluster 2 to calculate the distance between them. When calculating, the centers of the two concerned Si adatoms represent the boundaries of this distance, taking into account the number of vacant sites (N_s) between clusters 1 and 2 in a straight line

$$\text{distance} = d_{\mathrm{Si}} + N_s d_s. \tag{11}$$

Regarding d_s, the diameter of an empty site is estimated here to be equal to d_{Si}. Thus, (11) becomes

$$\text{distance} = d_{\mathrm{Si}}(N_s + 1). \tag{12}$$

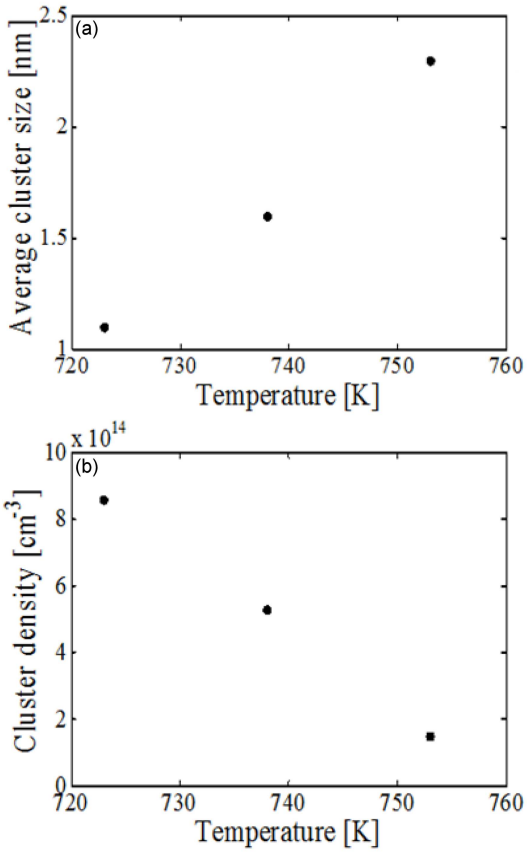

Fig. 9. Evolution of amorphous Si cluster size and density as a function of T.

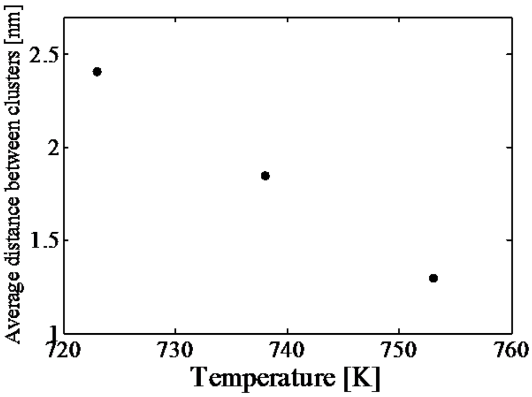

Fig. 10. Variation of the average distance between clusters with T.

Figure 12 exhibits deposited SiN_x films obtained with different T values. To clarify, enhancing T promotes coalescence phenomena within the structure, and consequently, the Si clusters come closer to each other by increasing their sizes and reducing the distance between them (with a decrease in N_s), as demonstrated in Fig. 12c.

The data confirm that this crucial input parameter significantly controls the determination of the morphologies of simulated nanostructures, i.e.,

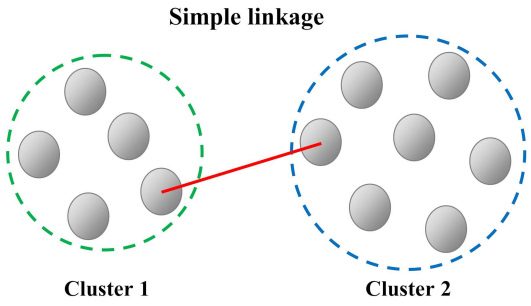

Fig. 11. Calculation of the average distance between Si clusters using the single linkage method.

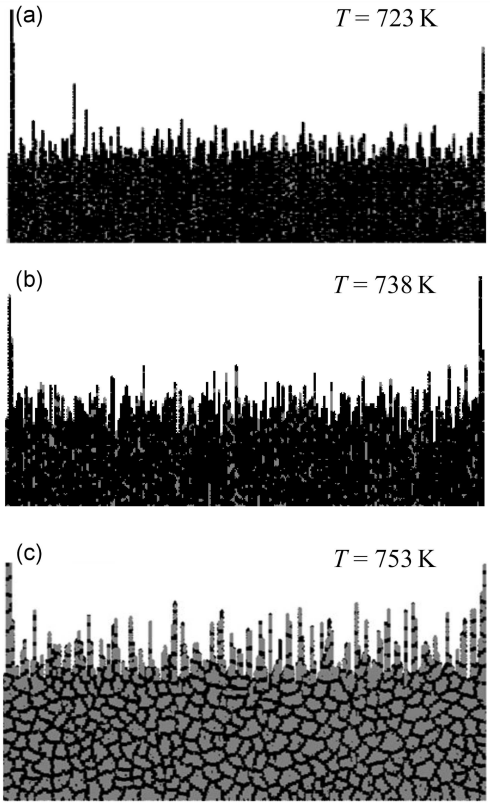

Fig. 12. SiN_x film nanostructures for different values of T.

film surface roughness. Whereas, with increasing T from 723 to 753 K, the surface roughness values of films increase, reaching its maximum at 753 K with 1.126 nm, as illustrated in Fig. 13. Obviously, this is attributed to the deposition of small amorphous Si clusters with high densities in the early stages of deposition [69].

Several authors have reported the effect of deposition temperature on the control of surface roughness during the deposition phase of SiN_x films [70–72]. The authors in [70] studied the characteristics of silicon nitride (SiN_x:H) films, grown by plasma-enhanced chemical vapor deposition (PECVD) on various metals such as Ta, IrMn, NiFe, Cu, and CoFe at different temperatures, using

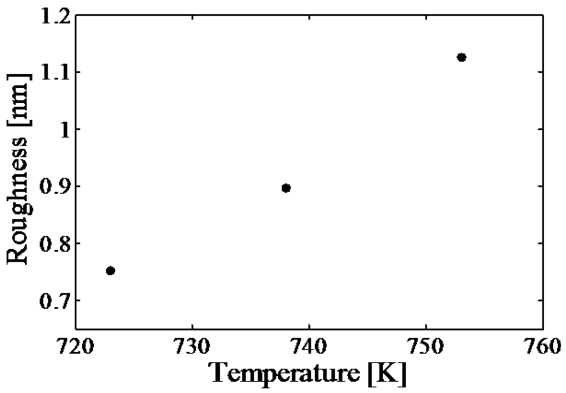

Fig. 13. Surface roughness for different values of T.

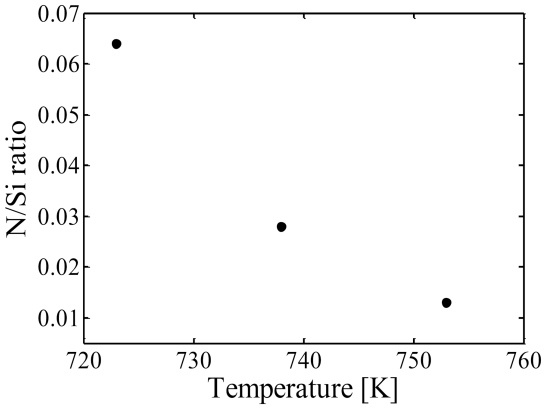

Fig. 14. SiN_x stoichiometry as a function of T.

measurements of buffered hydrofluoric acid (BHF) etch rate, surface roughness and Auger electron spectroscopy (AES). The researchers found that the surface of silicon nitride films deposited at lower temperatures (below 150°C) became rougher. However, at higher deposition temperatures (above 200°C), the SiN_x:H films exhibited low surface roughness values. Meanwhile, in [71], the authors presented studies on the surface morphologies and X-ray photoelectron spectroscopy (XPS) of metalorganic chemical vapor deposition (MOCVD)-grown SiN_x prepared under different conditions by variations of deposition temperature, the flow rate of SiH_4 source, and pre-nitridation conditions. Researchers confirmed that by employing an NH_3/SiH_4 flow rate of 2500/40 sccm, the surface roughness of SiN_x layers decreased from 0.91 nm to 0.17 nm with the increase in deposition temperature from 545 to 1035°C. Ahammou et al. in [72] explored the structural and mechanical properties of SiN_x thin films on SiO_2 substrates via molecular dynamics simulations. They revealed that both deposition temperature and energy significantly affected the surface roughness of SiN_x films. At 1100 K, the roughness values were consistently lower compared to 300 K, except in the case where the energy was 1 eV/atom and the Si/N ratio equaled 1, suggesting that higher temperatures facilitated smoother film growth due to enhanced atomic mobility.

To better explain the deposition of SiN_x films, a relationship between the different deposition parameters and the stoichiometry x is considered [58]

$$x = \frac{\mathrm{N}}{\mathrm{Si}} \approx 0.32 \frac{R}{V_{d_0}(T, P, \dots)}. \tag{13}$$

The N/Si ratio is directly related to the gas flow rate R (NH_3/Si_2H_6). Since ammonia NH_3 is responsible for the precipitation of N atoms by dissociative adsorption of SiH_2NH (see (7)), this ratio increases with R. According to this equation, the stoichiometry x also depends on the substrate temperature T, the total pressure P and the wafer-to-wafer distance, through V_{d_0}.

TABLE I

Silicon deposition rate V_0 and corresponding stoichiometry of SiN_x as a function of deposition temperature T.

Temperature T [K]	723	738	753
V_0 [nm/min]	1.5	3.4	7.3
N/Si ratio (x)	0.064	0.028	0.013

Since we use in this work a gas ratio R fixed at 0.3 with a pressure P equal to 26.66 Pa and a wafer-to-wafer distance of 20 mm, the stoichiometry x remains dependent only on the temperature T. Here and according to (1), the V_{d_0} factor is estimated equal to the pure disilane deposition rate V_0. Therefore, (13) becomes

$$x \approx \frac{0.096}{V_0(T)}. \tag{14}$$

The values of V_0 for the three adopted deposition temperatures [57] and those of the corresponding stoichiometry x are summarized in Table I.

From these results, we can deduce that the dependence of stoichiometry on temperature only occurs through V_0, which does not depend on the nitrogen content in the material. Moreover, as the adsorption phenomena of Si atoms are linked to the very reactive silylene molecule SiH_2 (see (6)), the increase in T leads to the decrease in the N/Si ratio for a given R, as shown in Fig. 14.

Overall, (6), (7), (9), and (13) allow us to determine and control the SiN_x film deposition kinetics, surface roughness, and stoichiometry as a function of all deposition parameters.

The results obtained here and in our previous work [56] constitute an important leap in the field of the formation and quality of SiN_x thin films. In fact, we found that the SiN_x morphological properties were very sensitive to different growth conditions. Thus, control of SiN_x deposition parameters is necessary to achieve the desired application. In [56], we observed that the gas flow rate has a significant effect on adjusting the roughness values

of the resulting films to those required. Meanwhile, in this work, we were able to predict the surface morphologies in terms of the size and density of Si clusters, the average distance between them, surface roughness, and stoichiometry as a function of the substrate temperature.

4. Conclusions

The dependence of surface roughness on substrate temperature during the LPCVD process of a SiN_x thin film on a three-dimensional triangular lattice was studied via our KMC algorithm. Two nanoscopic mechanisms were considered in the deposition process, i.e., the adsorption of NPs and the migration of Si adatoms (the desorption event was negligible, $P_{des} \sim 0$). A proposed model was employed to determine the morphologies of the obtained films in terms of the size and density of amorphous Si clusters as well as film surface roughness. The deposit was produced by alternating between Si and N atoms to form a SiN compound with small Si clusters. The migration of Si adatoms occurred either at the film surface or in the volume, resulting in a complementary event concerned with the evolution of pores and vacancies in the simulated structure. Indeed, the creation of peaks and valleys was described. The single linkage method was used to calculate the average distance between Si clusters. Surface roughness values were derived from the simulation matrix. The simulation results revealed that the process temperature intensely controlled the morphological evolution of the films, whether the film surface was smooth or rough. It was found that the N/Si ratio (SiN_x stoichiometry) depended only on temperature for a given gas ratio. This study established a direct relationship between deposition parameters and thin film nanostructures. Such data are crucial to motivate future innovations in the fields of microelectronics and photonics, where precise control of the morphological properties of thin films is essential.

References

[1] E. Ermakova, M. Kosinova, *J. Organomet. Chem.* **958**, 122183 (2022).

[2] N. Hegedüs, K. Balázsi, C. Balázsi, *Materials* **14**, 5658 (2021).

[3] R.E.I. Schropp, C.H.M. Van der Werf, V. Verlaan, J.K. Rath, H. Li, *Thin Solid Films* **517**, 3039 (2009).

[4] W. Xiong, H. Jiang, T. Li et al., *J. Mater. Sci. Mater. Electron.* **31**, 90 (2020).

[5] X. Wang, P. Wang, H. Yin, G. Zhou, R. Nötzel, *J. Electron. Mater.* **49**, 3577 (2020).

[6] S.X. Tao, A.M.M.G. Theulings, V. Prodanović, J. Smedley, H. Van der Graaf, *Computation* **3**, 657 (2015).

[7] S. Yoshinaga, Y. Ishikawa, Y. Kawamura, Y. Nakai, Y. Uraoka, *Mater. Sci. Semicond. Process.* **90**, 54 (2019).

[8] H. Nejadriahi, A. Friedman, R. Sharma, S. Pappert, Y. Fainman, P. Yu, *Opt. Express* **28**, 24951 (2020).

[9] A. Kuwabara, K. Matsunaga, I. Tanaka, *Phys. Rev. B* **78**, 064104 (2008).

[10] H.S. Dow, W.S. Kim, J.W. Lee, *AIP Adv.* **7**, 095022 (2017).

[11] T. Ohji, J. Tatami, *Ceram. Int.* **50**, 37282 (2024).

[12] K. Jhansirani, R.S. Dubey, M.A. More, S. Singh, *Results Phys.* **6**, 1059 (2016).

[13] C. Yang, J. Pham, *Silicon* **10**, 2561 (2018).

[14] R. Rodríguez-López, G. Soto-Valle, R. Sanginés, N. Abundiz-Cisneros, J. Águila-Muñoz, J. Cruz, R. Machorro-Mejía, *Thin Solid Films* **754**, 139313 (2022).

[15] L.Y. Beliaev, E. Shkondin, A.V. Lavrinenko, O. Takayama, *Thin Solid Films* **763**, 139568 (2022).

[16] E.S. Barrera-Mendivelso, A. Rodríguez-Gómez, *Front. Phys.* **11**, 1260579 (2023).

[17] B.B. Sahu, Y. Yin, J.G. Han, *Phys. Plasmas* **23**, 033512 (2016).

[18] L.K. Gautam, L. Ye, N. Podraza, *Surf. Sci. Spectra* **23**, 51 (2016).

[19] T. Iwahashi, M. Morishima, T. Fujibayashi, R. Yang, J. Lin, D. Matsunaga, *J. Appl. Phys.* **118**, 145302 (2015).

[20] J. Vallade, S. Pouliquen, P. Lecouvreur, R. Bazinette, E. Hernandez, S. Quoizola, *Energy Proc.* **27**, 365 (2012).

[21] Y. Lee, D. Gong, N. Balaji, Y.-J. Lee, J. Yi, *Nanoscale Res. Lett.* **7**, 50 (2012).

[22] C. Zhou, J. Zhu, S. Zhou, Y. Tang, S.E. Foss, H. Haug, Ř. Nordseth, E.S. Marstein, W. Wang, *Prog. Photovolt.* **25**, 23 (2017).

[23] Y. Sun, P. Gao, J. He, S. Zhou, Z. Ying, X. Yang, Y. Xiang, J. Ye, *Nanoscale Res. Lett.* **11**, 310 (2016).

[24] N.H. Nickel, W. Fuhs, H. Mell, W. Beyer, *MRS Online Proc. Libr.* **284**, 395 (2011).

[25] Y. Kuo, *Vacuum* **51**, 741 (1998).

[26] I. Parkhomenko, L. Vlasukova, F. Komarov, O. Milchanin, M. Makhavikou, A. Mudryi, V. Zhivulko, J. Żuk, P. Kopyciński, D. Murzalinov, *Thin Solid Films* **626**, 70 (2017).

[27] B. Rezgui, A. Sibai, T. Nychyporuk, M. Lemiti, G. Brémond, *J. Lumin.* **129**, 1744 (2009).

[28] D. Ge, Y. Zhang, H. Chen, G. Zhen, M. Wang, J. Jiao, L. Zhang, S. Zhu, *Mater. Design* **198**, 109338 (2021).

[29] B.S. Sheetz, Y.M.N.D.Y. Bandara, B. Rickson, M. Auten, J.R. Dwyer, *ACS Appl. Nano Mater.* **3**, 2969 (2020).

[30] Z.-B. Fan, Z.-K. Shao, M.-Y. Xie, X.-N. Pang, W.-S. Ruan, F.-L. Zhao, Y.-J. Chen, S.-Y. Yu, J.-W. Dong, *Phys. Rev. Appl.* **10**, 014005 (2018).

[31] T. Serdiuk, Y. Zakharko, T. Nychyporuk, A. Geloen, M. Lemiti, V. Lysenko, *Nanoscale* **4**, 5860 (2012).

[32] A.L. Aguayo-Alvarado, F.A. Araiza-Sixtos, N. Abundiz-Cisneros, R. Rangel-Rojo, K. Garay-Palmett, W. De La Cruz, *J. Non-Cryst. Solids* **613**, 122370 (2023).

[33] D. Bose, M.W. Harrington, A. Isichenko, K. Liu, J. Wang, N. Chauhan, Z.L. Newman, D.J. Blumenthal, *Light Sci. Appl.* **13**, 156 (2024).

[34] Z. Li, J. Jia, W. Jiang, W. Ou, B. Wang, X. Peng, H. Wu, Q. Zhao, *Mater. Sci. Semicond. Process.* **169**, 107868 (2024).

[35] C. Gong, W. Yang, S. Cheng, H. Zhang, Z. Yi, C. Ma, G. Li, Q. Zeng, R. Raza, *Mater. Today Commun.* **39**, 109229 (2024).

[36] N. Koompai, P. Limsuwan, X. Le Roux, L. Vivien, D. Marris-Morini, P. Chaisakul, *Results Phys.* **16**, 102957 (2020).

[37] J. Zhou, D. Al Husseini, J. Li, Z. Lin, S. Sukhishvili, G.L. Coté, R. Gutierrez-Osuna, P.T. Lin, *Sci. Rep.* **12**, 5572 (2022).

[38] P. Muñoz, G. Micó, L.A. Bru et al., *Sensors* **17**, 2088 (2017).

[39] A. Agarwal, N. Mudgal, A. Saharia, G. Singh, S.K. Bhatnagar, *Mater. Today Proc.* **66**, 3507 (2022).

[40] H. Hoi, S.S. Rezaie, L. Gong, P. Sen, H. Zeng, C. Montemagno, M. Gupta, *Biosens. Bioelectron.* **102**, 497 (2018).

[41] M.R. Bryan, J.N. Butt, J. Bucukovski, B.L. Miller, *ACS Sens.* **8**, 739 (2023).

[42] H.-K. Kim, S.-W. Kim, D.-G. Kim, J.-W. Kang, M.S. Kim, W.J. Cho, *Thin Solid Films* **515**, 4758 (2007).

[43] J.-A. Jeong, S.W. Jeong, N.-J. Park, J.-W. Kang, J.-K. Kim, D.-G. Kim, H.-K. Kim, *J. Electrochem. Soc.* **154**, J402 (2007).

[44] A. Kaloyeros, F. Jove, J. Goff, B. Arkles, *ECS J. Solid State Sci. Technol.* **6**, P691 (2017).

[45] D.A. Taher, M.A. Hameed, *Silicon* **15**, 7855 (2023).

[46] I. Guler, *Mater. Sci. Eng. B* **246**, 21 (2019).

[47] H.T.C. Tu, K. Ohdaira, *Jpn. J. Appl. Phys.* **63**, 01SP25 (2024).

[48] H. Zhou, C. Persson, W. Xia, H. Engqvist, *Mater. Res. Express* **10**, 115403 (2023).

[49] Z. Liu, S. Huang, Q. Bao et al., *J. Vac. Sci. Technol. B* **34**, 041202 (2016).

[50] A. Dubiel, G. Grabowski, M. Goły, S. Skrzypek, *Materials* **13**, 1092 (2020).

[51] S. Schmidt, T. Hanninen, J. Wissting, L. Hultman, N. Goebbels, A. Santana, M. Tobler, H. Hogberg, *J. Appl. Phys.* **121**, 171904 (2017).

[52] C.-L. Tien, T.-W. Lin, *Appl. Opt.* **51**, 7229 (2012).

[53] S.M.T. Mousavi, B. Hosseinkhani, C. Vieillard, M. Chambart, P.J.J. Kok, J.-F. Molinari, *Acta Mater.* **67**, 239 (2014).

[54] Y. Liu, N. Jehanathan, J.M. Dell, *J. Mater. Res.* **26**, 2552 (2011).

[55] W.J. Costakis Jr., C. Wyckoff, A. Schlup, M. Wallace, T. Craigs, E. Malek, A. Hilmas, L. Rueschhoff, *Addit. Manuf.* **64**, 103425 (2023).

[56] A. Bouhadiche, Z. Difellah, H. Bouridah, R. Remmouche, S. Benghorieb, M.R. Beghoul, S. Benzeghda, *Silicon* **15**, 5209 (2023).

[57] P. Temple-Boyer, B. Rousset, E. Scheid, *Thin Solid Films* **518**, 6897 (2010).

[58] P. Temple-Boyer, L. Jalabert, E. Couderc, E. Scheid, P. Fadel, B. Rousset, *Thin Solid Films* **414**, 13 (2002).

[59] A. Bouhadiche, H. Bouridah, N. Boutaoui, *Mater. Sci. Semicond. Process.* **26**, 555 (2014).

[60] D.R. Lide, *CRC Handbook of Chemistry and Physics*, CRC Press, Boca Raton (FL) 2005.

[61] J. Huang, G. Hu, G. Orkoulas, P.D. Christofides, *Chem. Eng. Sci.* **65**, 6101 (2010).

[62] I.S.S. Carrasco, T.B.T. To, F.D.A. Aarão Reis, *Phys. Rev. E* **108**, 064802 (2023).

[63] J. Huang, G. Orkoulas, P.D. Christofides, *Chem. Eng. Sci.* **94**, 44 (2013).

[64] N. Islam, D.C. Ghosh, *Open Spectrosc. J.* **5**, 13 (2011).

[65] K.S. Kim, K.H. Kim, Y.J. Ji, J.W. Park, J.H. Shin, A.R. Ellingboe, G.Y. Yeom, *Sci. Rep.* **7**, 13585 (2017).

[66] H. Bouridah, H. Haoues, M.R. Beghoul, F. Mansour, R. Remmouche, P. Temple-Boyer, *Acta Phys. Pol. A* **121**, 175 (2012).

[67] N.T.K. Thanh, N. Maclean, S. Mahiddine, *Chem. Rev.* **114**, 7610 (2014).

[68] J.A. Cortés, J.L. Palma, M. Wilson, *J. Volcanol. Geotherm. Res.* **165**, 163 (2007).

[69] P. Grammatikopoulos, M. Sowwan, J. Kioseoglou, *Adv. Theor. Simul.* **2**, 1900013 (2019).

[70] G.C. Han, P. Luo, K.B. Li, Z.Y. Liu, Y.H. Wu, *Appl. Phys. A* **74**, 243 (2002).

[71] Z. Fang, *Surf. Coat. Technol.* **202**, 4198 (2008).

[72] B. Ahammou, Y. Ouldhnini, A. Radi, B. Le Drogoff, K. Ghuman, M. Chaker, *Appl. Surf. Sci.* **680**, 161311 (2025).